sustainability

MDPI

Article

Laser-Induced Surface Vitrification for the Sustainable Stabilization of Copper Tailings

César Sáez-Navarrete [1,2,3,*], Xavier Baraza [4], Jorge Ramos-Grez [5], Carmen Sans [6], Claudia Arauzo [1] and Yoandy Coca [1]

[1] Department of Chemical and Bioprocess Engineering, School of Engineering, Pontificia Universidad Católica de Chile, Av. Vicuña Mackenna 4860, Macul, Santiago 7820436, Chile; cmarauzo@uc.cl (C.A.); ycoca@uc.cl (Y.C.)
[2] Research Center for Nanotechnology and Advanced Materials, Pontificia Universidad Católica de Chile, Av. Vicuña Mackenna 4860, Macul, Santiago 7820436, Chile
[3] Energy Center, Pontificia Universidad Católica de Chile, Av. Vicuña Mackenna 4860, Macul, Santiago 7820436, Chile
[4] Faculty of Economics and Business, Universitat Oberta de Catalunya, Rambla del Poblenou 156, 08018 Barcelona, Spain; jbaraza@uoc.edu
[5] Department of Mechanical and Metallurgical Engineering, School of Engineering, Pontificia Universidad Católica de Chile, Av. Vicuña Mackenna 4860, Santiago 8320165, Chile; jramos@uc.cl
[6] Department of Chemical Engineering and Analytical Chemistry, Faculty of Chemistry, Universitat de Barcelona, C/Martí i Franqués 1, 08028 Barcelona, Spain; carmesans@ub.edu
* Correspondence: csaezn@uc.cl

Abstract

This study introduces CO_2 laser surface vitrification as an innovative method for managing copper mining tailings, offering a sustainable solution to critical challenges in mineral processing. This technique transforms tailings into a stable and impermeable layer, immobilizing hazardous metals contained within them. By achieving vitrification at the surface level and operating at temperatures around 1200 °C, the process significantly reduces energy consumption compared to traditional vitrification methods, making it suitable for large-scale applications in remote mining sites. Detailed geochemical and mechanical analyses confirmed the formation of a dense vitreous matrix with high hardness (7.19–7.48 GPa) and reduced permeability, ensuring compliance with stringent environmental regulations. However, the brittle nature of the vitrified layer underscores the need for further research to enhance mechanical resilience. This work positions CO_2 laser vitrification as a transformative approach for integrating energy-efficient technologies into mineral processing, addressing key environmental concerns while advancing the sustainable management of mining waste.

Keywords: mining tailings; CO_2 laser vitrification; hazardous waste stabilization; sustainable mineral processing; environmental contamination control; energy-efficient technologies; tailings encapsulation

Academic Editor: Guannan Liu

Received: 19 April 2025
Revised: 13 June 2025
Accepted: 16 June 2025
Published: 20 June 2025

Citation: Sáez-Navarrete, C.; Baraza, X.; Ramos-Grez, J.; Sans, C.; Arauzo, C.; Coca, Y. Laser-Induced Surface Vitrification for the Sustainable Stabilization of Copper Tailings. *Sustainability* **2025**, *17*, 5676. https://doi.org/10.3390/su17135676

1. Introduction

Copper is among the most widely utilized metals in various sectors due to its excellent electrical and thermal conductivity. Consequently, the demand for copper mining has surged, particularly in Chile, where mining is a cornerstone of the economy, contributing 15% to the national GDP in 2023. Chile stands as the world's largest copper producer, holding approximately 24.7% of global copper reserves, equivalent to around 5328 thousand metric tons (2024).

One of the primary challenges associated with large-scale mining is managing the waste produced, known as tailings. Tailings are by-products of the mining process, comprising finely ground rock, water, and chemicals used in extraction [1,2]. These tailings pose significant environmental issues, necessitating responsible physical and chemical handling to prevent the release of toxic components into the environment. As of March 2023, Chile's Tailings Deposits Office reported 2131 tailings deposits. These were categorized as 292 active, 1679 inactive, and 160 abandoned. Most of these deposits are situated in the Coquimbo region (1128) and Atacama region (473), followed by Valparaíso (222), Antofagasta (146), and other regions (2024). This substantial amount of mining waste highlights the critical nature of this research. The geochemical composition of tailings is predominantly rock-forming elements, primarily oxides (silicon, aluminum, titanium, iron, calcium, magnesium, manganese, sodium, potassium, phosphorus, and sulfur), which are environmentally benign. However, 0.94% of these tailings include potentially toxic metals and metalloids such as copper, chromium, nickel, zinc, lead, arsenic, cadmium, and mercury. These elements can cause significant soil and water contamination if mobilized into the environment, with copper, lead, zinc, cadmium, and arsenic particularly problematic [3,4].

The current techniques for stabilizing tailings, such as water flooding [5] and impermeable isolation [6], have limitations. Additionally, polymeric substances have been employed as sealing and dust-retaining materials in mine tailings [7]. However, their primary disadvantage is the necessity for repeated application due to their limited temporary effectiveness, like wetting with water.

Vitrification is a well-established technology that transforms waste into a stable and homogeneous silicate glass through thermal fusion treatment. This process may also involve modifying the initial composition with glass-forming additives. These additives primarily include calcium, aluminum, and silicon oxides, which are key components of silicate glass and ceramics [8,9]. Vitrification transforms these wastes into glass or similar materials, effectively removing specific contaminants [10–12]. This process involves subjecting materials to high temperatures, typically between 1100 and 1400 °C, surpassing the glass transition temperature of their components. The resulting product is durable, has low porosity, and is resistant to leaching, making vitrification an attractive option for waste treatment [13,14]. Additionally, the silicate glass created during the vitrification process can be used as construction material, especially as a cementitious material [15].

Studies have shown that vitrification effectively stabilizes Cu-flotation waste, producing materials of high chemical durability [16]. Additionally, the vitrification of industrial sludges and waste has demonstrated the retention of metals such as Cr, Cu, Fe, Mn, Ni, and Zn in the glass matrix [17–21]. Also, adding certain additives can further improve the encapsulation of contaminants and reduce their leaching potential [22].

Immobilizing inorganic contaminants from industrial or mining waste is essential before land disposal or repurposing the waste [23–25].

Thermal treatment at lower firing temperatures (900–1400 °C) can effectively incorporate metal-containing waste materials into ceramic-stabilized products, allowing the volatilization of low-boiling-point compounds [26].

Given these advancements in waste stabilization, this research focuses on an innovative technique to further enhance the management of mining tailings. The goal of this research is to study the surface vitrification process of tailings using CO_2 laser spot melting. This method aims to develop an effective sealing and encapsulating technique for mining deposits by generating a thin, inert, and impermeable vitreous layer. This layer is designed

to cover the surface of tailings, thereby preventing erosion processes and minimizing environmental contamination.

2. Materials and Methods

2.1. Sample Collection

Three samples of inactive mining tailings were collected from the Andacollo commune in the Coquimbo region of Chile, where the primary resources extracted are gold and copper. Each sample, designated as M1, M2, and M3, was provided by the Chilean National Geology and Mining Service. The samples were manually homogenized through simple mixing to obtain representative samples of approximately 500 g of clayey-silty tailings.

2.2. Particle Size Estimation

Representative Scanning Electron Microscopy (SEM) micrographs of the untreated tailings samples (M1, M2, and M3) were analyzed to estimate particle size distributions. Image-based digital analysis was conducted using Python 3.11 and the OpenCV library. Particles were detected through binary thresholding and contour analysis, and their projected areas were calculated and converted into square micrometers (μm^2) using scale calibration based on the SEM image scale bars. This method provided a quantitative approximation of particle size distribution in the absence of conventional granulometric curves.

2.3. Chemical and Physical Characterization

Chemical and physical analyses were conducted on vitrified tailings samples (specimens) and non-vitrified samples (powdered tailings).

Initially, an elemental scan of eight common trace elements was performed using inductively coupled plasma mass spectrometry (ICP-MS) Agilent 7900 (Agilent Technologies, Santa Clara, CA, USA) following the standard method NCh-ISO17294/2:2016. The elements analyzed were Cu, Zn, Pb, As, Cr, Ni, Cd, and Hg, which are considered key environmental contaminants (CECs) associated with mining activities in Chile. These elements are prone to leaching, solubilization, and chemical reactions, potentially contaminating surface and groundwater.

To characterize the mineral phases, X-ray diffraction (XRD) analysis was conducted. The samples that were not sieved were placed uniformly on a sample holder and hand-pressed. A Bruker D8 Advance (Bruker Corporation, Billerica, MA, USA) diffractometer (graphite monochromator, with a CuKα1,2; Kβ X-ray tube, operating at 40 kV–40 mA, with a scanning range of 10–80°, a step size of 0.02°, and a measurement time of 2 s) was used. A semi-quantitative evaluation was performed using the EVA® software v3.1.

Additionally, the microstructural analysis, both physical and elemental, of the surface of the samples was conducted using Scanning Electron Microscopy (SEM) with energy-dispersive X-ray spectroscopy (EDS) JEOL JSM-IT500HR (JEOL Ltd., Tokyo, Japan) at 20 kV acceleration voltage. The surface of each sample was coated with gold.

Quantitative tests for the physical and chemical characterization of the samples were performed in triplicate, following the guidelines of the ISO/IEC 17025 standard in a DICTUC-certified laboratory.

2.4. Thermal Analysis

A simultaneous Thermogravimetric Analysis (TGA) and Differential Scanning Calorimetry (DSC) were performed on the three mining tailings samples to evaluate the effects of thermal treatment on phase decomposition. This analysis aimed to determine the optimal vitrification temperature, which must be set above the glass transition temperature (Tg) and the melting temperature (Tf).

Additionally, this analysis provided information on mass loss due to calcination, allowing the estimation of the percentage of potentially toxic elements volatilized during heating. The thermal profile of the tailings samples was obtained from heating curves, which are essential for controlling sintering processes in terms of both energy and mass transfer. This enables a more accurate prediction of the final vitreous product's quality.

The thermal analysis was conducted using a TA Instruments SDT-Q600 (TA Instruments, New Castle, DE, USA) simultaneous TGA/DSC system, operating with a nitrogen gas flow of 50 mL/min. Approximately 15 mg of each tailings sample was placed in 90 µL alumina crucibles, stabilized at 30 °C for 5 min, and subsequently heated to 1300 °C at a rate of 10 °C/min, simulating furnace conditions. The resulting thermal curves were analyzed, and characteristic temperatures were determined using TA Instruments' TA Analysis software, version 4.5A.

The thermal analyses were conducted using composite samples prepared from the original mining tailings samples M1, M2, and M3. Each composite sample was created by randomly combining equal portions from three replicate subsamples of the original tailings, ensuring a representative and homogeneous mixture.

2.5. Laser Vitrification Tests

Laser vitrification was performed using a CO_2 laser Synrad Firestar v30 (Synrad Inc., Mukilteo, WA, USA) with a power output of 30 W and a focal diameter of 0.32 mm.

Vitrified specimens were prepared from each of the mining tailings samples (M1, M2, and M3) using a controlled sintering process with a CO_2 laser. A standardized protocol was followed to ensure consistency and accuracy. The laser scanning path followed a predefined strategy to achieve uniform coverage and controlled melting of the surface (Figure 1).

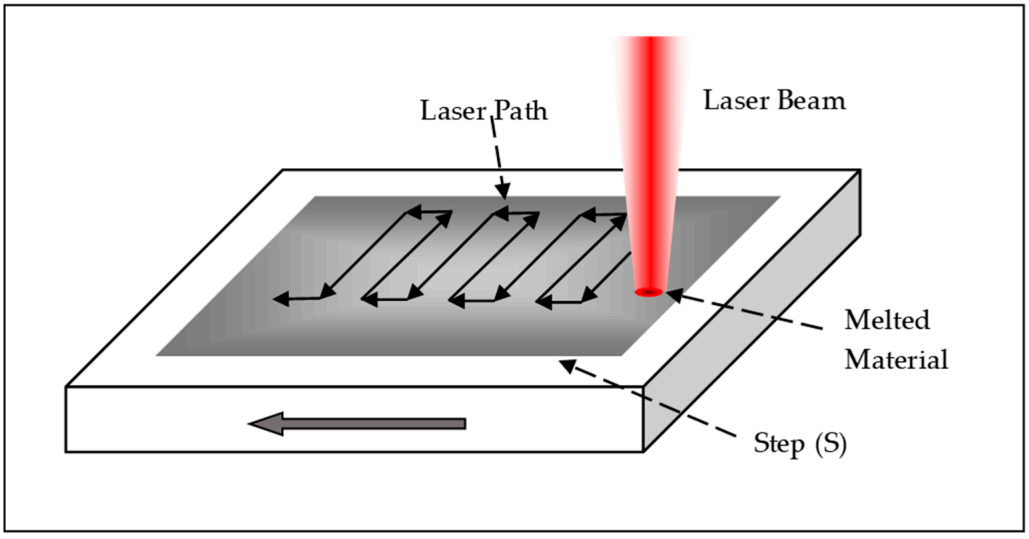

Figure 1. Laser path and melting process in tailings vitrification. Note: The arrows indicate the scanning direction of the CO_2 laser across the tailings surface.

The preparation process consisted of the following steps:

Sample Loading: Approximately 25 g of powdered tailings were placed into a container measuring $70 \times 30 \times 10$ mm^3. The material was evenly distributed to create a smooth surface, avoiding compression.

Sample Positioning: The container was precisely aligned within the CO_2 laser's incident area to ensure uniform exposure during sintering.

Laser Configuration: The experimental parameters, including laser power and scanning settings, were programmed into the control system according to the specifications outlined in Table 1.

Table 1. CO_2 laser parameters for surface vitrification of copper mining tailings.

CO_2 Laser Parameters	Value
Scanning Pattern S (°)	0
Laser Power (W)	23
Laser Step (mm)	0.15
Ambient Temperature (°C)	17
Specimen Dimensions (mm × mm)	60 × 10
Laser Focus Diameter (mm)	0.32
Relative Beam Speed (m/s)	0.007
Energy Supplied by Laser (J)	1.05
Vitrification Time per Specimen (min)	8
Energy Consumption (kWh/m^2)	5.11

Processing: The CO_2 laser was activated, and its power was adjusted to the predetermined level. This process resulted in the formation of vitrified specimens with final dimensions of 60 mm in length and 10 mm in width. The thickness was measured after completion.

Cooling and Labeling: The specimens were allowed to cool naturally to prevent thermal stress. Each was then labeled with the designation "LV" for laser vitrification, resulting in the following identifiers: LV-M1, LV-M2, and LV-M3.

2.6. Furnace Vitrification Tests

For furnace vitrification, a Carbolite Gero RHF 1200 muffle furnace (Carbolite Gero Ltd., Hope, UK) was used, with a maximum operating temperature of up to 1200 °C. Moreover, 10 × 10 mm^2 specimens were prepared using a furnace under the operational parameters outlined in Table 2. The target temperature of 1190 °C was selected based on the calorimetric analysis of the tailing samples (M1, M2, and M3). The preparation process involved placing each tailing sample into plaster molds, which served as disposable refractory containers specifically designed to form 10 × 10 mm^2 specimens. After filling the molds, the surface of the tailings was carefully smoothed to prevent compression. The molds were then introduced into the furnace, where the temperature gradually increased at a controlled rate of approximately 2 °C per minute. Once the target temperature was reached, it was maintained for 30 min to ensure complete vitrification. Finally, the specimens were allowed to cool gradually to prevent thermal stress and potential structural defects.

Table 2. Furnace parameters for vitrification of copper mining tailings.

Furnace Parameters	Value
Nominal Power (kW)	3
Nominal Temperature (°C)	1200
Heating Rate (°C/min)	2
Specimen Dimensions (mm × mm)	10 × 10
Vitrification Time per Specimen (min)	30
Energy Consumption (kWh/m^2)	2500

The vitrified specimens were labeled with the FV notation, indicating Vitrification with Furnace: FV-M1, FV-M2, and FV-M3.

It is important to note that special attention was given to temperature settings due to the potential exothermic reactions of certain tailings constituents, such as pyrite. To minimize the risk of damage to the molds, only small-scale specimens were prepared.

2.7. Mechanical Characterization

To evaluate the mechanical properties, a small-scale tensile testing device with a fracture force limit of <200 N was used to measure the tensile strength of laser-vitrified (LV) specimens with dimensions of 60 × 10 × 2 mm^3 (length × width × thickness). However, tensile testing could not be conducted on the furnace-vitrified (FV) specimens due to challenges in producing samples of the required size.

The hardness of the specimens was evaluated using a Vickers hardness test with a Mitutoyo HM-210 microhardness tester (Mitutoyo Corporation, Kawasaki, Japan). A 0.98 N load was applied using a diamond pyramid indenter to both laser-vitrified (LV) and furnace-vitrified (FV) specimens.

2.8. Leaching Tests

The effectiveness of the vitrification process in immobilizing heavy metals within the vitreous matrix was assessed through leaching tests following the SPLP EPA 1312 method, as specified in the EPA SW-846 standards under the Synthetic Precipitation Leaching Procedure (SPLP).

Laser-vitrified samples LV-M1, LV-M2, and LV-M3 were subjected to a leaching/extraction solution composed of concentrated sulfuric acid and nitric acid in a 60/40% weight ratio, diluted with water to achieve a pH of 5 ± 0.05. The volume of extractant used was 20 times the sample weight. The samples were placed on a rotary agitation system set at 120 rpm and agitated continuously for 54 h. After leaching, the concentrations of heavy metals in the filtered extract were analyzed using inductively coupled plasma mass spectrometry (ICP-MS) Agilent 7900 (Agilent Technologies, Santa Clara, CA, USA).

2.9. Simulated Infiltration Tests

A Mini Disk infiltrometer Model S (Decagon Devices Inc., Pullman, WA, USA) was used to evaluate the infiltration behavior of rainwater in superficially vitrified mining tailings compared to untreated tailings.

This instrument features a bubbling chamber that regulates water suction based on the texture of the sample. It measures the volume of water lost as it infiltrates the sample surface. In this study, 250 g samples of both laser-vitrified and untreated tailings were exposed to water flow from the infiltrometer, allowing for the determination of their hydraulic conductivities.

3. Results

3.1. Coupled Plasma Mass Spectrometry (ICP-MS)

The results of the inductively coupled plasma mass spectrometry (ICP-MS) analysis for the representative tailings samples M1, M2, and M3 are presented in Table 3. These concentrations were evaluated against the maximum permissible limits established for residential and industrial soils in countries with stringent environmental regulations, such as Canada, as well as against reference values reported for South American soils, including Brazil. The comparative analysis reveals that several elements in the tested samples exceed these international benchmarks. In the case of Chile, the absence of standardized regulatory thresholds for maximum allowable soil concentrations continues to pose a significant challenge for environmental risk assessment and contamination control.

Table 3. Principal metal and metalloid components in copper mine tailings targeted for vitrification.

Sample	Cu (µg/g)	Zn (µg/g)	Pb (µg/g)	As (µg/g)	Cr (µg/g)	Ni (µg/g)	Cd (µg/g)	Hg (µg/g)
M1	503.1 ± 10.1	1827.1 ± 54.8	97.4 ± 3.2	170.6 ± 5.1	53.9 ± 2.2	19.1 ± 1.0	6.37 ± 0.32	22.6 ± 1.1
M2	525.4 ± 11.0	500.8 ± 15.0	890.1 ± 35.6	71.1 ± 2.8	21.6 ± 1.1	3.43 ± 0.21	1.7 ± 0.09	2.27 ± 0.12
M3	524.1 ± 10.5	348.7 ± 11.2	495.2 ± 19.6	56.8 ± 2.3	20.3 ± 1.0	2.76 ± 0.18	3.1 ± 0.16	19.7 ± 0.98

3.2. X-Ray Diffraction (XRD) Analysis

The results of the mineralogical characterization, obtained through X-ray diffraction (XRD), are presented in Table 4. The primary minerals identified include quartz, low albite, low sanidine, calcite, and greenalite. Quartz is the predominant phase in samples M1 and M2, whereas in sample M3, albite is the most abundant mineral, comprising nearly 50% of the composition.

Table 4. Primary minerals present in the mine tailings samples selected for vitrification.

Name	Formula	M1 (%)	M2 (%)	M3 (%)
Quartz	SiO_2	43.3 ± 2.2	54.2 ± 2.7	21.5 ± 1.8
Albite	$Na(AlSi_3O_8)$	31.3 ± 1.9	38.3 ± 2.3	45.9 ± 2.7
Sanidine	$(K_{0.93}Na_{0.07})(AlSi_3O_8)$	16.9 ± 1.4	4.9 ± 0.6	25.8 ± 1.8
Calcite	$CaCO_3$	7.1 ± 0.7	1.8 ± 0.3	6.5 ± 0.6

3.3. SEM and EDS Spectral Analysis

Morphological analysis of the untreated tailings samples revealed a distinctly heterogeneous particle size distribution. M1 exhibited the largest particle aggregates, with a maximum area of 4.36×10^6 µm^2 and a standard deviation of ±642,652 µm^2, indicating high dispersion. M2 and M3 showed lower mean particle areas of 18,118 µm^2 and 6848 µm^2, respectively, but all three samples had median areas around 300 µm^2 and similar minimum values of approximately 63 µm^2. Interquartile ranges fell between 143 and 1190 µm^2. Despite this variability, more than 75% of particles in each sample displayed areas below 1000 µm^2, suggesting a predominance of fine-grained material interspersed with larger fragments. These findings confirm the heterogeneous granular nature of the tailings, which may affect thermal response, sintering behavior, and vitrification performance. EDS spectral analysis confirmed the predominant presence of silicon oxides and aluminosilicates. In sample M1, minerals primarily composed of Al-Si-O were identified, along with particles rich in iron and sulfur, likely corresponding to pyrite. Sample M2 predominantly contains minerals with Fe-Si-O composition, suggesting the presence of iron silicates and oxides. For sample M3, EDS analysis confirmed a majority presence of Al-Si-O, likely associated with aluminosilicates. Additionally, elements with high Fe-O content were easily detectable on the surface (Figure 2).

M1

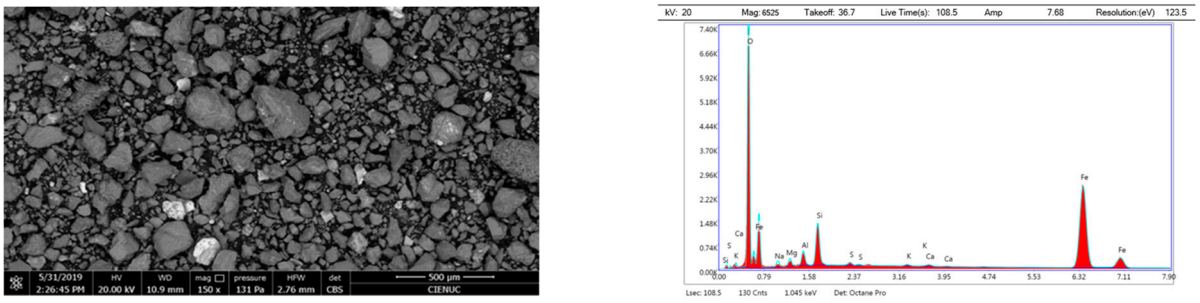

Figure 2. *Cont.*

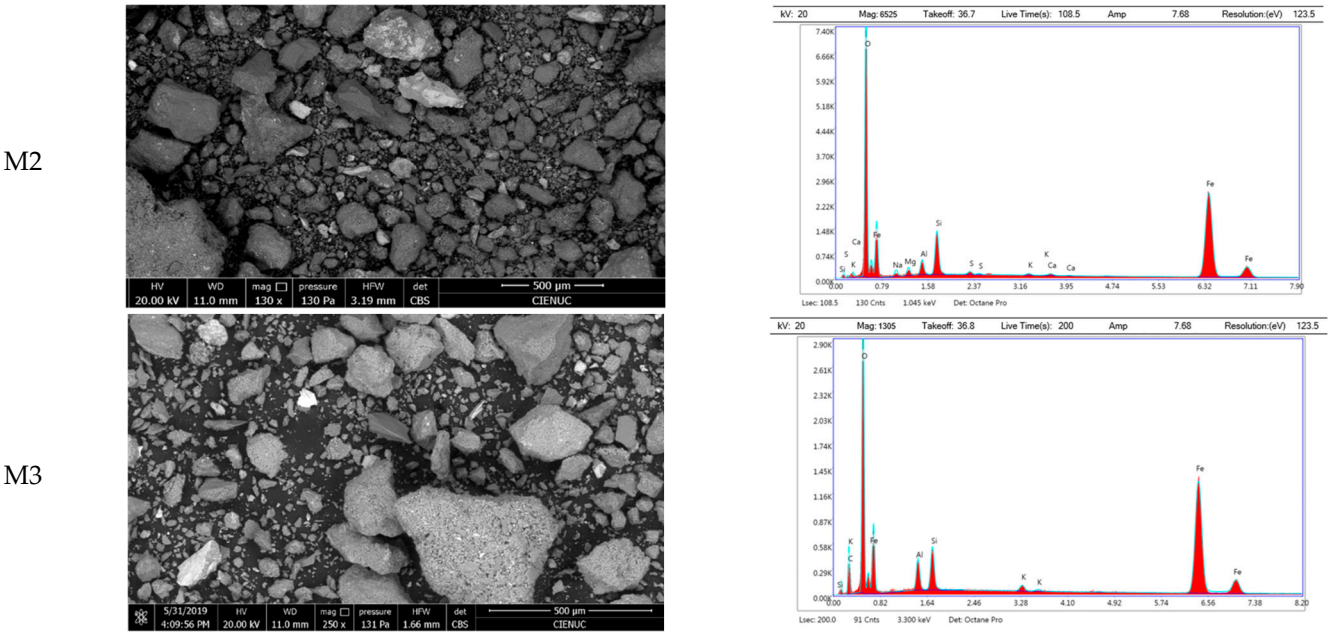

Figure 2. Scanning Electron Microscopy (SEM) images and corresponding Energy Dispersive X-ray Spectroscopy (EDS) spectra of the untreated copper tailings samples: M1 (top row), M2 (middle row), and M3 (bottom row). SEM images highlight morphological differences, while EDS confirms predominant Al-Si-O and Fe-rich phases. (middle row), and M3 (bottom row). SEM images highlight morphological differences, while EDS confirms predominant Al-Si-O and Fe-rich phases.

3.4. Results of Thermal Analysis

The thermal analysis results for samples M1, M2, and M3 are presented in Figure 3. All three samples exhibit similar multi-stage decomposition patterns with comparable thermal behavior, likely due to their compositional similarities.

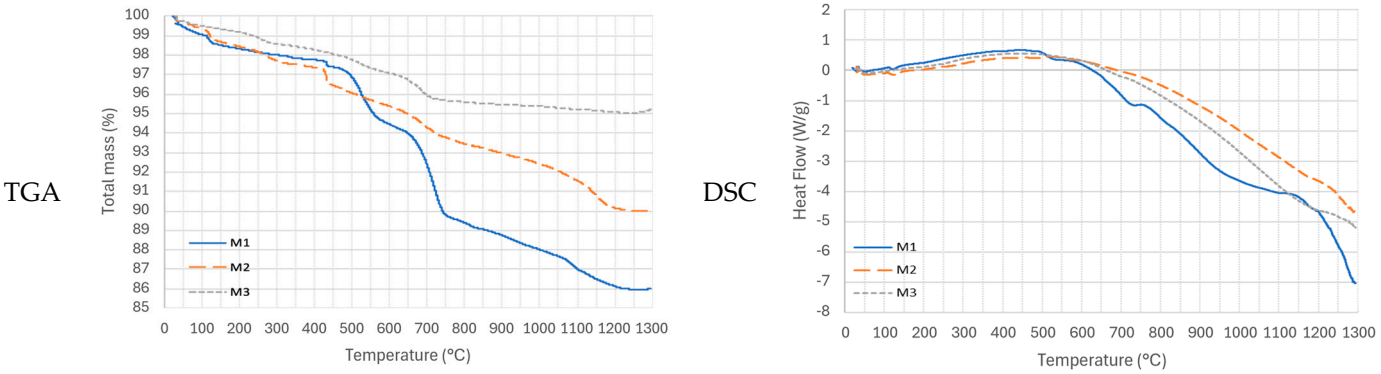

Figure 3. Thermal analysis of composite tailings samples (M1, M2, and M3) using Thermogravimetric Analysis (TGA) and Differential Scanning Calorimetry (DSC). The TGA curve represents mass loss during heating, while DSC reveals glass transition, crystallization, and fusion points relevant to vitrification.

An initial endothermic peak between 100 and 150 °C suggests minor dehydration in 3all samples. At 430 °C, a mass loss event, accompanied by an endothermic heat flow signal, is observed, corresponding to the glass transition temperature [27,28].

A common endothermic peak between 450 and 650 °C is associated with the transformation of greenalite (a mineral present in all three samples and belonging to the kaolinite group) due to the dehydroxylation of hydroxides or the loss of the hydroxyl group [29,30].

A second endothermic peak between 650 and 750 °C indicates a crystallization temperature with a mass loss of less than 5%. The final endothermic peak, observed between

1100 and 1200 °C, corresponds to the fusion phase of the samples, aligning with studies that report fusion peaks around 1160 °C [27–29].

Above 1200 °C, the thermal curves stabilize, indicating the absence of further mass loss due to calcination. Based on these results, the optimal thermal treatment temperature is set above the fusion point, specifically at 1200 °C for laser treatment and furnace treatment.

It is important to highlight the limited availability of comprehensive databases on the thermal behavior of mining tailings, as well as the inherent complexity of interpreting thermal curves due to the heterogeneous mineral composition. However, the observed results and comparisons between different tailings reveal a consistent pattern, enabling the identification of key thermal events such as glass transition, crystallization, and fusion.

3.5. Results of Laser Vitrification Tests

The laser incidence temperature on the tailings samples was measured using a pyrometer, reaching an average maximum of 1200 °C, which is consistent with the temperature defined in the thermal analysis. Figures 4 and 5 present SEM micrographs of vitrified samples M1, M2, and M3 treated by laser (LV) and furnace (FV) vitrification, highlighting differences in surface morphology and microstructural evolution depending on the technique applied.

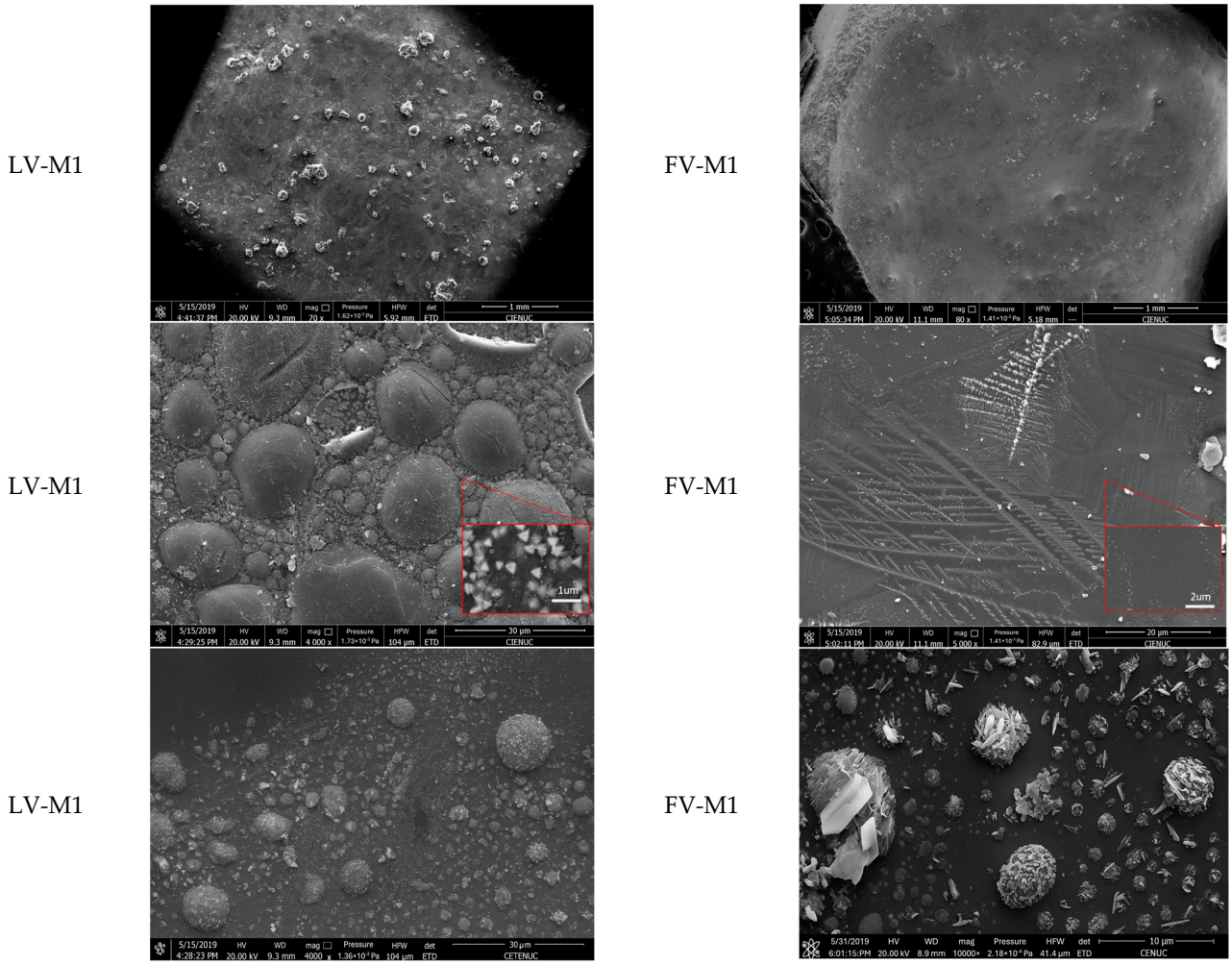

Figure 4. Scanning Electron Microscopy (SEM) images of vitrified M1 samples treated by laser-induced surface vitrification (LV) and furnace vitrification (FV) at various magnifications. Differences in microstructure highlight the morphological effects of each vitrification technique.

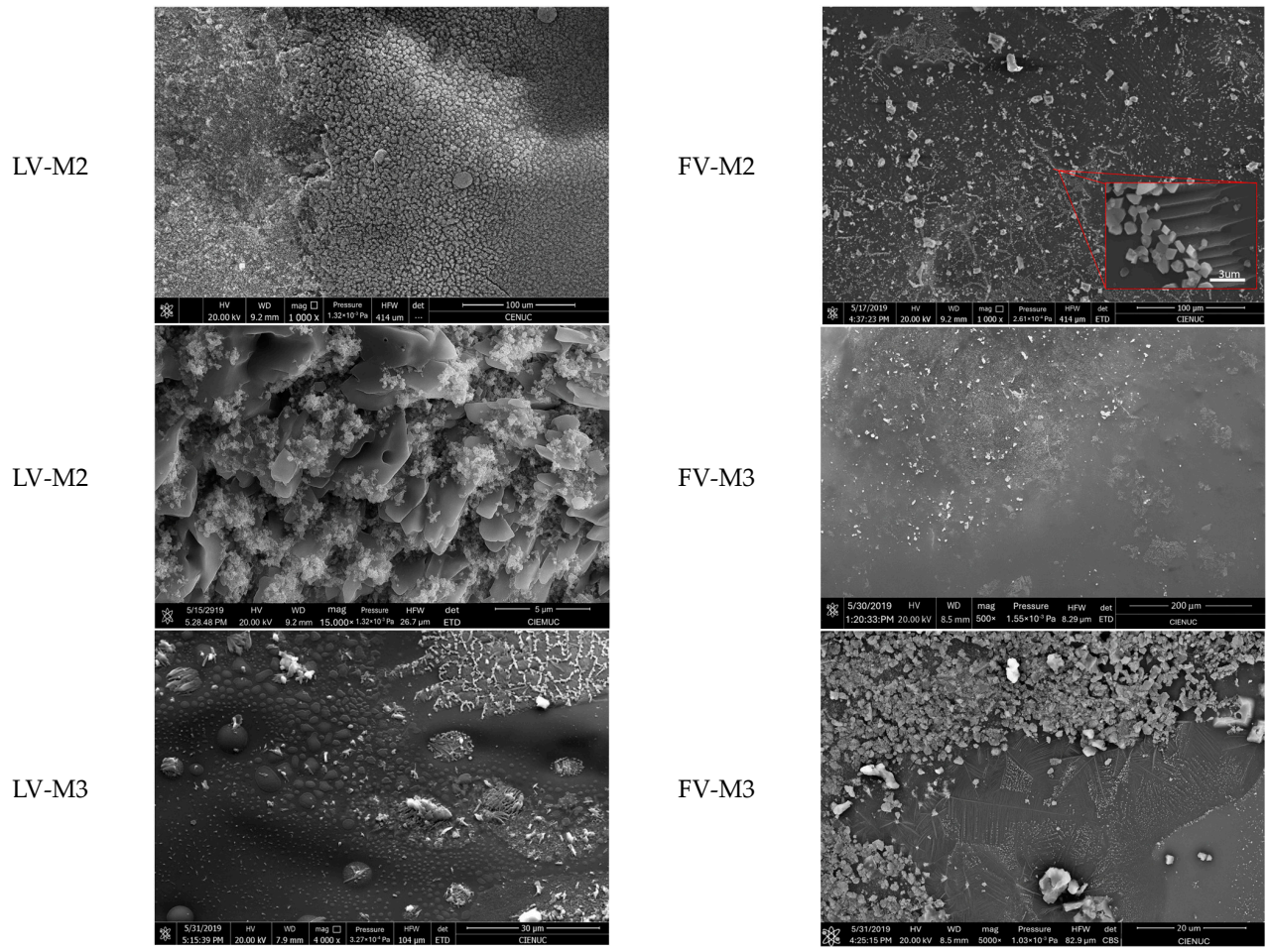

Figure 5. SEM micrographs of the surface vitrification process induced by CO_2 laser (LV) and by furnace heating (MV) at different magnifications for vitrified samples M2 and M3.

The results for the three tailings samples are summarized in Table 5, with specimens measuring 60 × 10 mm^2 and an average thickness of 2 mm.

Table 5. Metal and metalloid components in M1, M2, and M3 copper mine tailings post CO_2 laser vitrification.

Sample	Cu (µg/g)	Zn (µg/g)	Pb (µg/g)	As (µg/g)	Cr (µg/g)	Ni (µg/g)	Cd (µg/g)	Hg (µg/g)
LV-M1	448.89 ± 9.0	1359.09 ± 41.0	81.42 ± 3.3	84.48 ± 3.0	65.57 ± 2.6	17.86 ± 0.9	2.27 ± 0.11	0.57 ± 0.03
LV-M2	512.73 ± 10.3	422.05 ± 12.7	728.39 ± 29.1	41.64 ± 1.7	20.89 ± 0.8	2.7 ± 0.14	1.08 ± 0.05	1.45 ± 0.07
LV-M3	664.06 ± 13.3	264.06 ± 7.9	395.46 ± 15.8	25.23 ± 1.0	18.67 ± 0.7	1.77 ± 0.09	1.63 ± 0.08	0.43 ± 0.02

Elemental characterization was performed using ICP-MS Agilent 7900 (Agilent Technologies, Santa Clara, CA, USA) to determine the concentrations of Cu, Zn, Pb, As, Cr, Ni, Cd, and Hg.

3.6. Results of Furnace Vitrification Tests

The results of the vitrification process using the furnace (muffle) are presented in Table 6. Data for the furnace-vitrified sample M1 (FV-M1) could not be obtained due to repeated structural failures of the gypsum mold. The mold was unable to withstand the intense exothermic reactions generated during the vitrification process, leading to its collapse and the loss of the sample in multiple trials. The elemental composition of furnace-vitrified samples (FV-M2 and FV-M3) was quantified using ICP-MS, as detailed in Section 2.3.

Table 6. Metal and metalloid components in M1, M2, and M3 copper mine tailings post furnace vitrification.

Sample	Cu (µg/g)	Zn (µg/g)	Pb (µg/g)	As (µg/g)	Cr (µg/g)	Ni (µg/g)	Cd (µg/g)	Hg (µg/g)
FV-M1	-	-	-	-	-	-	-	-
FV-M2	466.34 ± 9.3	804.79 ± 24.1	903.06 ± 36.1	47.77 ± 1.9	19.23 ± 0.8	9.4 ± 0.5	0.94 ± 0.05	0.62 ± 0.03
FV-M3	389.43 ± 7.8	518.01 ± 15.5	428.07 ± 17.1	23.26 ± 0.9	21.21 ± 0.8	7.16 ± 0.4	1.59 ± 0.08	0.19 ± 0.01

3.7. Results of Mechanical Characterization

Mechanical properties, including tensile strength and microhardness, were assessed as described in Section 2.7. The results are summarized below.

Laser-vitrified samples exhibited an average tensile strength of 0.1 MPa, indicating a brittle nature of the resulting vitreous material. This low strength limits its application in dynamic environments where mechanical loads or structural integrity are critical. At the same time, no comparable datasets exist for vitreous ceramics derived from mining tailings; studies on laser-sintered powders with metallic content report significantly higher tensile strengths (above 40 MPa). The brittleness observed in this study underscores the need for further optimization, such as the addition of reinforcing additives or modifications in the vitrification process to enhance mechanical performance.

Hardness measurements were conducted using a Vickers microhardness tester, applying a 0.98 N load with a diamond pyramid indenter. The vitrified samples exhibited high hardness values, with 7.19 GPa for laser-vitrified (LV) specimens and 7.48 GPa for furnace-vitrified (FV) specimens. These values are comparable to hardened steel and commercial vitreous ceramics [29], making the material highly resistant to abrasion and surface wear. The rapid heating and cooling associated with CO_2 laser vitrification likely contributed to the enhanced rigidity of the material, while the metallic components present on the surface, such as aluminosilicates and ferric oxides, further reinforced the hardness.

While the high hardness of the vitrified material is advantageous for static applications, such as capping tailings deposits, its brittleness restricts its use in dynamic or load-bearing scenarios. Future research should focus on improving tensile strength by exploring composite formulations or alternative vitrification techniques. Additionally, long-term studies on wear resistance under field conditions would provide valuable insights into its applicability for large-scale mining operations.

3.8. Results of Leaching Tests

The SPLP leaching test was conducted only on the samples obtained by laser vitrification (LV) due to the difficulty in obtaining FV samples with the appropriate dimensions. The results are shown in Table 7 below.

Table 7. Metal concentration (µg/L) results from leaching tests of CO_2 laser-vitrified samples LV-M1, LV-M2, and LV-M3.

Sample ID	Cu (µg/L)	Zn (µg/L)	Pb (µg/L)	As (µg/L)	Cr (µg/L)	Ni (µg/L)	Cd (µg/L)	Hg (µg/L)
LV-M1-LIX	4.17 ± 0.17	340.79 ± 10.2	0.94 ± 0.04	122.57 ± 4.9	8.1 ± 0.3	<0.9	1.7 ± 0.08	<5.34
LV-M2-LIX	5.72 ± 0.23	172.02 ± 5.2	1.27 ± 0.05	65.29 ± 2.6	<2.44	<0.9	<0.62	<5.34
LV-M3-LIX	20.23 ± 0.81	118.62 ± 3.6	1.86 ± 0.07	59.96 ± 2.4	5.45 ± 0.2	<0.9	0.63 ± 0.03	<5.34
Chl. Std.	-	-	5	5	5	-	1	200
EU Std.	30,000	15	3	300	2.5	3	300	30

Leaching tests on LV samples were conducted using the SPLP method, following the protocol detailed in Section 2.8. Table 7 presents the results.

The samples were subjected to an acidic extractant at a pH of 5 ± 0.05, with a sample-to-solution ratio of 1:20 by weight. The procedure included extended agitation at 120 rpm

for 54 h to evaluate the robustness of the vitrified matrix under extreme conditions. Post-leaching, metal concentrations in the extract were quantified using inductively coupled plasma mass spectrometry (ICP-MS) Agilent 7900 (Agilent Technologies, Santa Clara, CA, USA).

The results demonstrated the exceptional performance of the vitrified samples in immobilizing toxic metals. All metal concentrations in the leachates were well below the regulatory limits established by Chilean hazardous waste guidelines (Chl. Std.) and the European Directive 1999/31/EC (EU Std.). Notably, lead (Pb) and arsenic (As), which are typically highly leachable, exhibited minimal concentrations in all samples. The low leachability of these elements highlights the effectiveness of the glassy matrix formed during laser vitrification in containing hazardous substances [31].

These findings confirm the potential of CO_2 laser vitrification as a sustainable and efficient method for mitigating the environmental risks associated with mining tailings. The process ensures compliance with stringent environmental standards, making it an attractive solution for mining waste stabilization. Future studies should investigate the long-term performance of the vitrified materials under variable environmental conditions to further validate their durability and effectiveness.

3.9. Results of Simulated Infiltration Tests

Infiltration behavior was evaluated using the Mini Disk infiltrometer, as outlined in Section 2.9. The results below highlight differences in hydraulic conductivity.

The results showed a significant reduction in permeability for the vitrified samples. While untreated tailings exhibited an average hydraulic conductivity of k ~4.85×10^{-4} cm/s, the laser-vitrified samples demonstrated near-impermeability, with k < 1×10^{-7} cm/s. These values indicate that the vitrified layer effectively prevents water infiltration and the associated mobilization of toxic metals. This impermeability makes the vitrified material a suitable barrier for applications such as tailings pond capping, particularly in regions prone to acid rain or other forms of precipitation.

The findings confirm the utility of CO_2 laser vitrification as an effective technique for minimizing the environmental risks associated with water infiltration in mining tailings. Future studies could explore long-term durability under variable climatic conditions to further validate its applicability in large-scale mining operations.

4. Discussion

The analysis of copper tailings revealed significant variability in metal and metalloid concentrations, with Cu, Zn, Pb, and As as the predominant elements. These differences reflect site-specific factors, such as ore type and extraction methods, highlighting the need for tailored management approaches.

SiO_2 was the primary mineral in M1 and M2, consistent with previous studies on copper slag and mine tailings [32–34]. XRD and SEM confirmed high levels of aluminosilicates and silicon oxides, while ICP-MS validated the presence of quartz, albite, and iron silicate minerals, which influence vitrification and contaminant immobilization.

Thermal analysis identified key transitions, including dehydration, dehydroxylation, crystallization, and fusion, with a melting point around 1190–1200 °C. These parameters guided laser and furnace vitrification. Previous studies have shown that higher temperatures increase the glass content in metal waste [35], emphasizing the importance of precise thermal control.

Vitrification tests confirmed that both CO_2 laser and furnace-based treatments effectively immobilized toxic metals. Leaching analyses revealed that post-treatment concentrations of Cu, Zn, Pb, and As were well below regulatory thresholds, with laser-treated

samples achieving near-complete immobilization [36]. However, the vitrified products exhibited low tensile strength (~0.1 MPa), indicating significant brittleness. Despite this, their hardness values (7.19–7.48 GPa) are comparable to those of commercial vitreous ceramics. Mechanical performance is known to vary depending on both composition and processing conditions, as reported in studies involving hematite and quartz-rich tailings [37,38].

To better understand the disparity between hardness and tensile strength, the relationship between mineralogical composition and mechanical behavior was further examined. XRD and SEM-EDS analyses indicated that samples M1 and M2 are dominated by aluminosilicate phases, such as quartz and feldspars. While these minerals contribute to increased hardness, they also tend to form brittle, glassy matrices, particularly under rapid cooling. This explains the observed mechanical profile of laser-vitrified samples, where fast surface vitrification may induce residual stresses and microcracking. In contrast, furnace vitrification allows for slower and more uniform thermal gradients, facilitating atomic rearrangement and stress relaxation. This potentially enhances structural cohesion despite similar mineralogical content. These findings highlight the combined influence of both phase composition and thermal kinetics on the mechanical integrity of vitrified tailings.

To address the low tensile strength observed in vitrified samples, future research should explore compositional modifications aimed at improving mechanical resilience. One promising strategy involves the use of calcium-rich additives (e.g., CaO or $CaCO_3$), which can promote the formation of crystalline phases that enhance structural strength and crack resistance. In addition, incorporating ceramic reinforcements such as alumina (Al_2O_3) or zirconia (ZrO_2) has proven effective in increasing fracture toughness in similar glass–ceramic systems. Other approaches, including fiber or particulate reinforcement and the optimization of cooling rates to reduce residual stresses, should also be considered. These techniques may enable the development of vitrified materials with improved tensile performance, thereby expanding their potential applications in structural or encapsulation contexts.

Laser vitrification offers advantages due to rapid heating and localized treatment, but its high energy consumption poses challenges for large-scale implementation. Integrating renewable energy, such as solar power, could improve sustainability. Infiltration tests showed near-zero permeability ($k < 1 \times 10^{-7}$ cm/s), making vitrified material ideal for encapsulating metals in tailings storage facilities and reducing environmental risks.

Scanning Electron Microscopy (SEM) analysis of vitrified samples (Figures 4 and 5) reveals distinct morphological characteristics between laser vitrification (LV) and furnace vitrification (FV). In laser-treated samples, the surface is marked by heterogeneity, microbubbles, and embedded mineral phases. These features are indicative of rapid surface vitrification, where intense thermal gradients lead to partial melting and localized encapsulation of elements. Notably, the presence of microbubbles suggests gas retention, potentially offering an additional mechanism for trapping volatile compounds. In contrast, furnace-vitrified samples exhibit a smoother and more homogeneous surface, with fewer surface crystallization but more extensive internal mineral growth. These differences reflect the nature of thermal input: laser treatment produces a high-temperature gradient over a short time, promoting glassy surfaces with superficial crystalline structures, while furnace treatment allows deeper and more uniform heat diffusion, favoring internal phase development and densification. Although SEM surface analysis indicates higher crystalline content in LV samples, XRD analysis confirms that the overall crystallinity is significantly higher in FV specimens. This suggests that LV promotes surface-limited crystallization with an otherwise amorphous matrix, whereas FV fosters bulk crystallization. These microstructural distinctions are essential for understanding the encapsulation behavior and mechanical

properties of vitrified products, and they support the development of tailored vitrification strategies based on specific environmental and operational requirements.

Although post-vitrification leaching tests indicated low residual mercury concentrations (<5.34 μg/L), the potential volatilization of low-boiling-point metals such as mercury remains a valid concern. The thermal treatments used in this study, particularly laser vitrification, may generate localized high-temperature zones that could facilitate volatilization, even if not detectable under small-scale conditions. Therefore, future studies should incorporate gas-phase monitoring during vitrification processes, particularly in scaled-up systems, to quantify possible metal emissions. Such data would be essential for evaluating the environmental safety and regulatory compliance of industrial vitrification technologies applied to mine tailings.

In terms of energy efficiency, laser surface vitrification consumes 5.11 kWh/m^2, significantly less than deep-melting vitrification, making it viable for remote mining sites with high energy costs. However, its low mechanical strength limits applications in load-bearing structures. Future research should explore additives or composite materials to enhance mechanical performance without compromising contaminant encapsulation.

5. Conclusions

This study demonstrates that CO_2 laser surface vitrification is an innovative and energy-efficient technique for managing copper mining tailings, addressing critical challenges in the mineral processing industry. By transforming tailings into a stable, impermeable vitreous layer, this method effectively immobilizes hazardous metals such as copper, lead, and arsenic, ensuring compliance with stringent environmental regulations.

The key innovation of this technique lies in its superficial vitrification approach, which drastically reduces energy consumption compared to conventional deep-melting vitrification methods. Operating at approximately 1200 °C, this process is particularly suited for large-scale applications in remote or energy-constrained mining sites. The ability to generate a dense glassy matrix with high hardness (7.19–7.48 GPa) and minimal permeability highlights its potential for long-term containment of toxic elements, mitigating environmental contamination risks associated with tailings storage.

Despite its success in stabilizing hazardous materials, the brittle nature of the vitrified layer suggests that further research is required to enhance its mechanical resilience for broader industrial applications. Potential improvements could include the incorporation of reinforcing additives or modifications to the vitrification process to increase the material's structural strength without compromising its environmental performance.

The scalability and energy efficiency of CO_2 laser vitrification positions it as a transformative technology for the mining sector. Its integration with renewable energy sources, such as solar or wind power, offers a pathway for further reducing operational costs and environmental impact. By advancing waste management practices, this innovation has the potential to redefine sustainable mining waste management globally.

6. Patents

The work reported in this manuscript is related to the Chilean invention patent titled "Material para impermeabilización compuesto por una capa vitrificada y una capa cementicia elaborado con materiales obtenidos de relaves mineros y métodos" (Invention Patent No. 366-2020). The patent was filed under application number CL201902860 on 7 October 2019, and was granted in 2020. It describes a waterproofing material composed of a vitrified layer and a cementitious layer, both derived from mining tailings, along with the associated methods for its production.

Author Contributions: Conceptualization, C.S.-N.; methodology, C.S.-N., C.S., X.B. and J.R.-G.; software, Y.C.; validation, C.S.-N., C.S. and X.B.; formal analysis, C.A.; investigation, C.A.; resources, C.S.-N.; data curation, C.S.-N., C.S. and X.B.; writing—original draft preparation, C.A., Y.C. and C.S.-N.; writing—review and editing, C.S.-N.; visualization, Y.C. and C.S.-N.; supervision, C.S.-N., C.S., X.B. and J.R.-G.; project administration, C.S.; funding acquisition, C.S.-N. All authors have read and agreed to the published version of the manuscript.

Funding: This study was supported by internal funding from the Laboratory of Renewable Energy and Waste, Pontificia Universidad Católica de Chile.

Institutional Review Board Statement: Not applicable.

Informed Consent Statement: Not applicable.

Data Availability Statement: The data supporting the findings of this study are included within the article.

Acknowledgments: The authors would like to thank the support of colleagues who contributed to logistical arrangements and access to experimental facilities. During the preparation of this manuscript, the authors used ChatGPT (OpenAI, version April 2024) for the purposes of grammar and spelling corrections in English. The authors have reviewed and edited the output and take full responsibility for the content of this publication.

Conflicts of Interest: The funders had no role in the design of the study; in the collection, analysis, or interpretation of data; in the writing of the manuscript; or in the decision to publish the results.

Abbreviations

The following abbreviations are used in this manuscript:

GDP	Gross Domestic Product
LV	Laser-vitrified sample
FV	Furnace-vitrified sample
ICP-MS	Inductively Coupled Plasma Mass Spectrometry
XRD	X-ray Diffraction
SEM	Scanning Electron Microscopy
EDS	Energy-Dispersive X-ray Spectroscopy
TGA	Thermogravimetric Analysis
DSC	Differential Scanning Calorimetry
SPLP	Synthetic Precipitation Leaching Procedure
CEC	Contaminant of Environmental Concern
Tg	Glass Transition Temperature
Tf	Fusion Temperature
Chl. Std.	Chilean standard hazardous waste guidelines
EU Std.	European Directive 1999/31/EC

References

1. Reyes-Bozo, L.; Herrera-Urbina, R.; Escudey, M.; Godoy-Faúndez, A.; Sáez-Navarrete, C.; Herrera, M.; Ginocchio, R. Role of biosolids on hydrophobic properties of sulfide ores. *Int. J. Miner. Process.* **2011**, *100*, 124–129. [CrossRef]
2. Reyes-Bozo, L.; Higueras, P.; Godoy-Faúndez, A.; Sobarzo, F.; Sáez-Navarrete, C.; Vásquez-Bestagno, J.; Herrera-Urbina, R. Assessment of the floatability of chalcopyrite, molybdenite and pyrite using biosolids and their main components as collectors for greening the froth flotation of copper sulphide ores. *Miner. Eng.* **2014**, *64*, 38–43. [CrossRef]
3. He, Z.L.L.; Yang, X.E.; Stoffella, P.J. Trace elements in agroecosystems and impacts on the environment. *J. Trace Elem. Med. Biol.* **2005**, *19*, 125–140. [CrossRef] [PubMed]
4. Yu, Y.T.; Qu, G.F.; Wu, B.; Lu, Q.L.; Ning, P. Characterization of the Stabilization of Arsenic in Mine Tailings. *Anal. Lett.* **2017**, *50*, 1862–1875. [CrossRef]
5. Komárek, M.; Vanek, A.; Ettler, V. Chemical stabilization of metals and arsenic in contaminated soils using oxides—A review. *Environ. Pollut.* **2013**, *172*, 9–22. [CrossRef]

6. Johnson, D.B.; Hallberg, K.B. Acid mine drainage remediation options: A review. *Sci. Total Environ.* **2005**, *338*, 3–14. [CrossRef]
7. Chen, Q.Y.; Tyrer, M.; Hills, C.D.; Yang, X.M.; Carey, P. Immobilisation of heavy metal in cement-based solidification/stabilisation: A review. *Waste Manag.* **2009**, *29*, 390–403. [CrossRef]
8. Perret, D.; Sierk, A.; Machado, N.P.; Agullo, J.; Laplace, A.; Bardez-Giboire, I.; Hugon, I. Crystallization and rheology of Na_2O-CaO-Al_2O_3-SiO_2 melt in the vitrification of technological waste. *Int. J. Appl. Glass Sci.* **2024**, *15*, 227–242. [CrossRef]
9. Hossain, M.U.; Xuan, D.X.; Poon, C.S. Sustainable management and utilisation of concrete slurry waste: A case study in Hong Kong. *Waste Manag.* **2017**, *61*, 397–404. [CrossRef]
10. Aloisi, M.; Karamanov, A.; Taglieri, G.; Ferrante, F.; Pelino, M. Sintered glass ceramic composites from vitrified municipal solid waste bottom ashes. *J. Hazard. Mater.* **2006**, *137*, 138–143. [CrossRef]
11. Cheng, L.C.; Wu, S.H.; Huang, K.L.; Lin, C.T.; Wang, C.T.; Wang, J.W.; Kuo, Y.M. Evaluation of effect of reducing additives during vitrification via simulation and experiment. *J. Air Waste Manag. Assoc.* **2013**, *63*, 1182–1189. [CrossRef] [PubMed]
12. Cubas, A.L.V.; Machado, M.D.; Machado, M.D.; Dutra, A.R.D.; Moecke, E.H.S.; Fiedler, H.D.; Bueno, P. Final treatment of spent batteries by thermal plasma. *J. Environ. Manag.* **2015**, *159*, 202–208. [CrossRef]
13. Meng, F.; Wu, Z.; Wang, Q.; Du, J.; Deng, H.; Liu, X.; Lin, Z. Parameter relationship and product characteristics analysis of heavy-metal hazardous wastes vitrification under the combination of data science and experiment. *J. Environ. Chem. Eng.* **2024**, *12*, 112408. [CrossRef]
14. Sanito, R.C.; Bernuy-Zumaeta, M.; You, S.-J.; Wang, Y.-F. A review on vitrification technologies of hazardous waste. *J. Environ. Manag.* **2022**, *316*, 115243. [CrossRef] [PubMed]
15. Lake, D.J. In-flight vitrification of granitic aggregate: Characterization and performance of a scalable supplementary cementitious material. *Constr. Build. Mater.* **2023**, *409*, 133980. [CrossRef]
16. Li, C.T.; Lee, W.J.; Huang, K.L.; Fu, S.F.; Lai, Y.C. Vitrification of chromium electroplating sludge. *Environ. Sci. Technol.* **2007**, *41*, 2950–2956. [CrossRef]
17. Garcia-Valles, M.; Avila, G.; Martinez, S.; Terradas, R.; Nogués, J.M. Heavy metal-rich wastes sequester in mineral phases through a glass-ceramic process. *Chemosphere* **2007**, *68*, 1946–1953. [CrossRef]
18. Kuo, Y.M.; Wang, C.T.; Tsai, C.H.; Wang, L.C. Chemical and physical properties of plasma slags containing various amorphous volume fractions. *J. Hazard. Mater.* **2009**, *162*, 469–475. [CrossRef]
19. Dellisanti, F.; Rossi, P.L.; Valdrè, G. In-field remediation of tons of heavy metal-rich waste by joule heating vitrification. *Int. J. Miner. Process.* **2009**, *93*, 239–245. [CrossRef]
20. Wang, Q.; Yan, J.H.; Chi, Y.; Li, X.D.; Lu, S.Y. Application of thermal plasma to vitrify fly ash from municipal solid waste incinerators. *Chemosphere* **2010**, *78*, 626–630. [CrossRef]
21. Wang, H.-Y.; Hou, Y.; Zhang, G.-H.; Chou, K.-C. Valuable metals recovery and vitrification of chromium-containing electroplating sludge. *Metall. Res. Technol.* **2022**, *119*, 402. [CrossRef]
22. Chou, I.C.; Wang, Y.F.; Chang, C.P.; Wang, C.T.; Kuo, Y.M. Effect of NaOH on the vitrification process of waste Ni-Cr sludge. *J. Hazard. Mater.* **2011**, *185*, 1522–1527. [CrossRef] [PubMed]
23. Singh, I.B.; Chaturvedi, K.; Morchhale, R.K.; Yegneswaran, A.H. Thermal treatment of toxic metals of industrial hazardous wastes with fly ash and clay. *J. Hazard. Mater.* **2007**, *141*, 215–222. [CrossRef]
24. Almendro-Candel, M.B.; Vidal, M.M.J. Glasses, Frits and Glass-Ceramics: Processes and Uses in the Context of Circular Economy and Waste Vitrification. *Coatings* **2024**, *14*, 346. [CrossRef]
25. Navarro, A.; Cardellach, E.; Corbella, M. Immobilization of Cu, Pb and Zn in mine-contaminated soils using reactive materials. *J. Hazard. Mater.* **2011**, *186*, 1576–1585. [CrossRef]
26. Careghini, A.; Dastoli, S.; Ferrari, G.; Saponaro, S.; Bonomo, L.; De Propris, L.; Gabellini, M. Sequential solidification/stabilization and thermal process under vacuum for the treatment of mercury in sediments. *J. Soils Sediments* **2010**, *10*, 1646–1656. [CrossRef]
27. Lay, G.F.T.; Rockwell, M.C.; Wiltshire, J.C.; Ketata, C. Characteristics of silicate glasses derived from vitrification of manganese crust tailings. *Ceram. Int.* **2009**, *35*, 1961–1967. [CrossRef]
28. Pegolo, P.; Grasselli, F. Thermal transport of glasses via machine learning driven simulations. *Front. Mater.* **2024**, *11*, 1369034. [CrossRef]
29. Liu, J.; Ding, L.; Wang, Q.; Luo, L.; Wang, H. Recycling of arsenic residue to basalt fiber via vitrification. *Ceram. Int.* **2024**, *50*, 36622–36630. [CrossRef]
30. Taylor-Lange, S.C.; Lamon, E.L.; Riding, K.A.; Juenger, M.C.G. Calcined kaolinite-bentonite clay blends as supplementary cementitious materials. *Appl. Clay Sci.* **2015**, *108*, 84–93. [CrossRef]
31. Conte, S.; Molinari, C.; Ardit, M.; Mantovani, L.; Tribaudino, M.; Cruciani, G.; Dondi, M.; Zanelli, C. Hazardous element inertisation in vitrified silicate ceramics: Effect of different matrices. *J. Hazard. Mater.* **2024**, *474*, 134657. [CrossRef]
32. Shi, C.; Meyer, C.; Behnood, A. Utilization of copper slag in cement and concrete. *Resour. Conserv. Recycl.* **2008**, *52*, 1115–1120. [CrossRef]

33. Esmaeili, J.; Al-Mwanes, A.O. Production of eco-friendly UHPC with high durability and resistance to harsh environmental conditions using copper mine tailings. *J. Build. Eng.* **2023**, *76*, 107297. [CrossRef]
34. Simonsen, A.M.T.; Solismaa, S.; Hansen, H.K.; Jensen, P.E. Evaluation of mine tailings' potential as supplementary cementitious materials based on chemical, mineralogical and physical characteristics. *Waste Manag.* **2020**, *102*, 710–721. [CrossRef] [PubMed]
35. Huang, R.; Zhou, S.; Chen, J.; Zeng, X.; Han, Y.; Qin, J.; Huang, Y.; Lin, F.; Yu, X.; Liao, S.; et al. A novel method for efficiently recycling platinum group metals and copper by Co-smelting spent automobile catalysts with waste-printed circuit boards. *J. Clean Prod.* **2024**, *447*, 141517. [CrossRef]
36. Drif, B.; Taha, Y.; Hakkou, R.; Benzaazoua, M. Integrated valorization of silver mine tailings through silver recovery and ceramic materials production. *Miner. Eng.* **2021**, *170*, 107060. [CrossRef]
37. Chen, Y.; Zhang, Y.; Chen, T.; Zhao, Y.; Bao, S. Preparation of eco-friendly construction bricks from hematite tailings. *Constr. Build. Mater.* **2011**, *25*, 2107–2111. [CrossRef]
38. Lemougna, P.N.; Yliniemi, J.; Ismailov, A.; Levanen, E.; Tanskanen, P.; Kinnunen, P.; Roning, J.; Illikainen, M. Recycling lithium mine tailings in the production of low temperature (700–900 °C) ceramics: Effect of ladle slag and sodium compounds on the processing and final properties. *Constr. Build. Mater.* **2019**, *221*, 332–344. [CrossRef]